Seasonal variability of phytoplankton vertical distribution in a contrasted South Pacific Ocean from BioGeoChemical-Argo profiling floats

T. Hermilly[1], E. Martinez[1], J. Uitz[2], M. Cornec[3,4], N. Kolodziejczyk[1] and C. Schmechtig[5]

[1]Laboratoire d'Océanographie Physique et Spatiale (LOPS), UMR 6523, IUEM, Université de Bretagne Occidentale, Brest, IRD, CNRS, Ifremer, Plouzané, France

[2]Laboratoire d'Océanographie de Villefranche (LOV), UMR 7093, CNRS, Sorbonne Université, Villefranche-sur-mer, France.

[3]School of Oceanography University of Washington, Seattle, WA, USA

[4]NOAA/OAR Pacific Marine Environmental Laboratory, Seattle, WA, USA

[5]OSU Ecce Terra, UAR 3455, CNRS, Sorbonne Université, Paris Cedex, France.

Corresponding author: Thomas Hermilly (thomas.hermilly@ird.fr)

Key Points:

- We report contrasted seasonal variations of phytoplankton vertical distribution in the undersampled South Pacific from 13 BGC-Argo floats
- In oligotrophic gyres, subsurface biomass influenced by stratification below the mixed layer may have been largely underestimated
- Equatorial waters show unique chlorophyll profiles, with a pronounced subsurface peak and a persistent surface bloom feature

Abstract

The seasonal variability of phytoplankton vertical distribution is investigated in the South Pacific where observations are scarce and scattered. We used 13 BioGeoChemical-Argo floats deployed across diverse oceanic environments. The seasonal latitudinal displacement of the Tasman front induces transitions from mesotrophic to oligotrophic conditions. This shift results in Chlorophyll-a concentration vertical distribution changing from bloom types to Subsurface Chlorophyll Maxima (SCM) types, with intermediate hybrid types between these extremes. Such hybrid profiles frequently occur in the equatorial Pacific, highlighting a large-scale pattern rather than local island mass effect. In oligotrophic regions, seasonal variations of light availability and stratification dynamics below the mixed layer likely relate SCMs to an increase in carbon biomass or photoacclimation. A biomass increase is frequently observed, contrary to previously reported, suggesting that subsurface phytoplankton production may have been largely underestimated. This calls for further observations of the water column in these remote undersampled open ocean areas.

Plain Language Summary

This study investigates the seasonal variability in the vertical distribution of Chlorophyll-a concentration (Chl, a proxy of phytoplankton biomass) in the South Pacific. We use observations from autonomous platforms (BioGeoChemical-Argo floats) deployed in nutrient-limited (oligotrophic) areas (center of the gyre, Tonga area and Coral Sea), the mesotrophic equatorial area and the Tasman Sea. In oligotrophic regions, a permanent maximum of Chlorophyll at depth (or Subsurface Chlorophyll Maximum, SCM) shows seasonal changes, likely due to either a biomass increase or physiological adaptation to light conditions. Mixing and water column destabilisation help bring nutrients to the SCM layer, promoting biomass increase. The Tasman front, which delineates oligotrophic conditions northward and mesotrophic ones southward. In this area Chl vertical profiles appear to be seasonally representative of oligotrophic or mesotrophic dynamics with SCM and bloom types, respectively, according to the seasonal position of the front. Finally, the high occurrence of Hybrid (combining SCM and bloom) type profiles in the equatorial area appears to be related to the regional environment rather than to the effects of surrounding islands. These findings highlight the need for further studies in remote, nutrient-limited regions of the open ocean.

1 Introduction

Phytoplankton, at the basis of the marine food web, play a key role for the oceanic upper trophic levels and carbon export to the deep ocean. Hence, it is essential to characterise the spatio-temporal variability of their biomass. Phytoplankton growth relies on the availability of light and nutrients, the latter being made available in the sunlit layer through oceanic and atmospheric processes. Specifically, changes in the water column stratification due to vertical mixing can induce the uplift of nutrients from the deep ocean to the euphotic zone, hence allowing phytoplankton to grow (e.g. Eppley et al., 1979; Gačić et al., 2002; Peeters et al., 2013). Conversely, intense stratification, such as in the oligotrophic gyres, prevents nutrient uplift (e.g. Lewis et al., 1986; Moore et al., 2013; Strom & Fredrickson, 2008) in which case phytoplankton are confined to a deeper layer of the water column, at a depth where the amount of available light and nutrients is balanced (Cullen, 2015; Morel et al., 2010). Such subsurface maxima are well-documented through observations of Chlorophyll-a concentration (Chl), a proxy for phytoplankton biomass. They are referred to as Deep Chlorophyll Maxima (DCM) or Subsurface Chlorophyll Maxima (SCM; e.g., Cullen, 2015; Shulenberger & Reid, 1981). Albeit widely used, Chl is nevertheless an ambiguous proxy, as the Chl-to-carbon biomass ratio depends on phytoplankton composition and physiology and, in particular, changes with depth due to the physiological response of phytoplankton cells to light-limited conditions, a process called photoacclimation (Geider, 1987). Hence, SCM distributions do not always reflect a concomitant increase in Chl and carbon biomass at depth (i.e. Subsurface Biomass Maxima, SBM), but instead an increase of Chl associated with photoacclimation (i.e. Subsurface Acclimation Maxima, SAM; e.g. Barbieux et al., 2019; Cornec et al., 2021). The latter being likely associated with reduced biological production in oligotrophic environments (e.g. Barbieux et al., 2022), the distinction between these two processes is crucial to study the biological carbon pump and ecosystem dynamics (e.g. Westberry et al., 2008). However, environmental processes triggering SAM and SBM remain poorly understood, at the seasonal scale in particular.

The vast South Pacific Ocean (SPO) encompasses a variety of biogeochemical environments. It hosts the largest oligotrophic area of the global ocean, with strong stratification inducing relatively low mean surface Chl (< 0.1 $mg.m^{-3}$; Claustre & Maritorena, 2003; Morel et al., 2010;

Figure 1a). This area itself is contrasted, ranging from moderate oligotrophy in the western tropical SPO ($\simeq$ 0.1 mg.m^{-3}) to extreme oligotrophy ($\simeq$ 0.01 mg.m^{-3}) in the vicinity of Easter Island (Claustre et al., 2008). Observations from few oceanic cruises in the South Pacific Subtropical Gyre (SPSG) have revealed spatial differences in the subsurface layer considering the depth and intensity of the SCM, but also the composition of phytoplankton communities (Bonnet et al., 2023; Claustre et al., 2008; Moutin et al., 2017; Ras et al., 2008). In addition, only two studies focused on the investigation of the seasonal variability of Chl vertical distributions in this region, using only one year of observations from a BioGeoChemical-Argo (BGC-Argo) profiling float each (Mignot et al., 2014; Sauzède et al., 2020). However, how this seasonal variability is modulated along a longitudinal gradient in the oligotrophic SPSG, as well as the relative importance of SAM vs. SBM and the underlying physical and biogeochemical processes have never been investigated.

The oligotrophic SPSG is surrounded by mesotrophic environments along the equatorial band as well as at temperate and high latitudes. North of the SPSG, the equatorial divergence induces High Nutrient Low Chlorophyll (HNLC) conditions (Murray et al., 1992) which may be disturbed by the presence of islands such as the Marquesas Islands (Martinez & Maamaatuaiahutapu, 2004). Observations based on one oceanographic cruise and one year deployment of a BGC-Argo float allowed the investigation of the vertical structure of Chl within this archipelago in 2011-2012 (Martinez et al., 2020). The Chl vertical profiles appeared to alternate between well-mixed distributions (i.e., homogeneous distribution of Chl in the mixed layer) and a combination of well-mixed and SCM patterns along a north-south gradient. However the authors could not specify whether the Chl vertical distribution combining these two types of profiles was induced by particular biogeochemical properties of the HNLC area or by the presence of the islands (Island Mass Effect, IME; Doty & Oguri, 1956), nor by some regional and/or seasonal forcings.

At temperate latitudes at the SPO western boundary, the Tasman Sea straddles the Tasman Front, which represents an eastern extension of the East Australian Current. This current separates from the east coast of Australia at a seasonal scale (Kerry & Roughan, 2020) and meanders towards the northern tip of New Zealand (Oke et al., 2019). North of the front, the

stratified, oligotrophic Coral Sea waters are relatively unproductive, while the vertically well-mixed waters south of the front exhibit strong biological activity (Baird et al., 2008). Studies on phytoplankton based on in-situ observations focused on the North-East Tasman Sea (Ellwood et al., 2013) or on the western region close to the Australian East coast (e.g., Baird et al., 2008; Suthers et al., 2011). Within the Tasman Sea, only two satellite based studies have investigated the Chl variability at a seasonal scale but observations were limited to the surface (Chiswell et al., 2013; Tilburg et al., 2002). Importantly, here again, the seasonal variability of the vertical dynamics of Chl at the scale of the Tasman front remains unclear.

Over the last decade, the BGC-Argo program has drastically increased the number of in-situ measurements of key physical and biogeochemical variables, in particular in remote, poorly sampled regions like the SPO. Recent studies based on this program investigated the seasonal variability of Chl vertical distributions at the global scale (Bock et al., 2022; Cornec et al., 2021), the North Atlantic Ocean (Lacour et al., 2019) or the Mediterranean Sea (Barbieux et al., 2019). In contrast, a specific focus on the SPO has never been performed, so that the seasonal variability of the Chl vertical distribution in this basin remains largely unknown, as well as the physical-biogeochemical processes at stake. Here, we use observations from 13 BGC-Argo profiling floats that drifted from 2015 to 2023 in the contrasted SPO provinces presented above (Figure 1a and b), namely the temperate-latitude Tasman Sea (T_{Tasman}), the equatorial HNLC area (E_{HNLC}), and three oligotrophic regions following a zonal gradient from the Coral Sea (O_{Coral}), the Fiji-Tonga region (O_{Fiji}) toward the center of the SPSG (O_{center}). The aim of the present study is to characterise the seasonal variability of the Chl vertical distribution in these regions and to investigate the underlying physical-biogeochemical mechanisms. A focus is placed on the SAM and SBM seasonality along the east-west gradient of the SPSG.

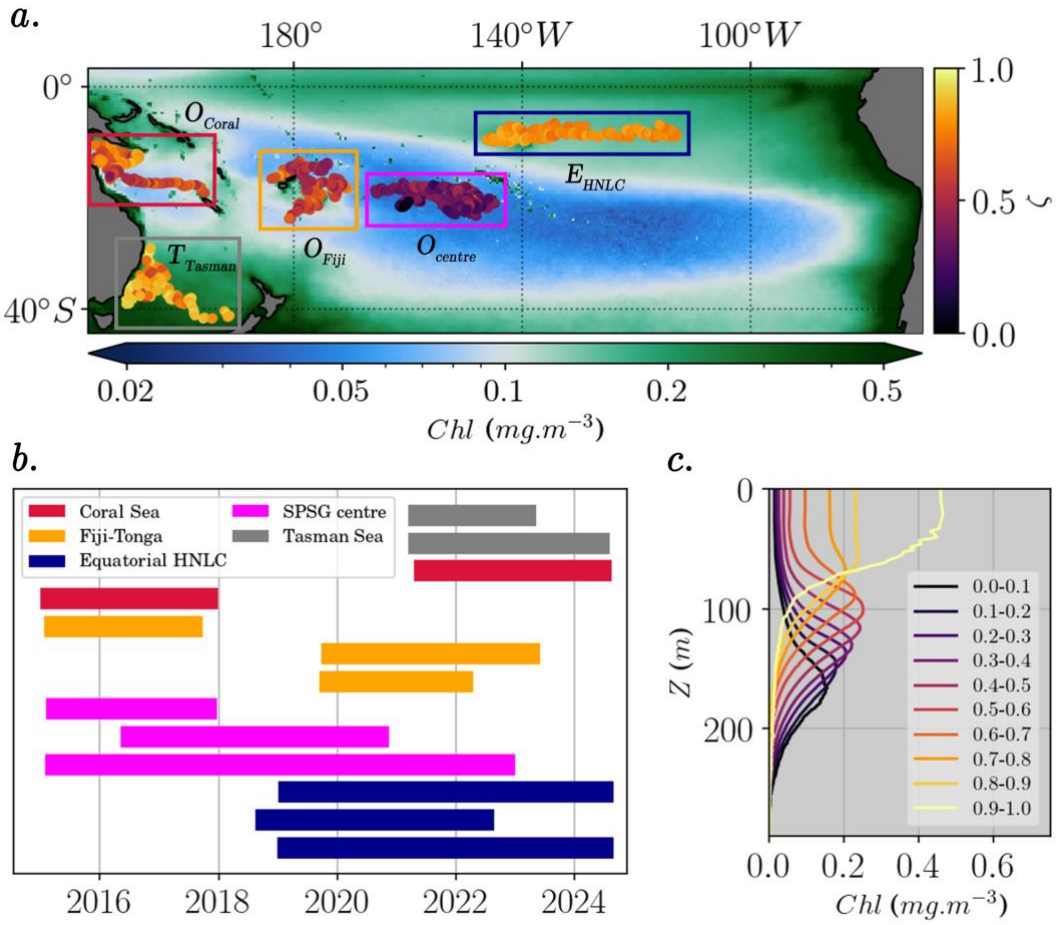

Figure 1. (a) Trajectories of the 13 BGC-Argo floats. Each dot represents the location of a float profile with its ζ value in colour as presented in (c). ζ is an indicator of the shape of the Chl vertical profile (vertical colorbar). Boxes delineate the five distinct regions of float drift, namely the Tasman Sea (T_{Tasman}), the Coral Sea (O_{Coral}), the Fiji-Tonga region (O_{Fiji}), the center of the South Pacific Subtropical Gyre (O_{center}) and the equatorial HNLC area (E_{HNLC}). The colour in background is the surface Chl from the OC-CCI satellite product averaged over 2015-2023 (horizontal colorbar). (b) Timeline of Chl measurements for each BGC-Argo float, with colours corresponding to float drift regions as in (a). (c) Range of ζ values corresponding to the Chl vertical profiles. The associated Chl values are indicated as the X-axis.

2 Data and Methods

2.1 Processing of the BGC-Argo measurements

We use observations from 13 BGC-Argo profiling floats (Figure 1a and b), deployed in the Tasman and Coral Seas, the vicinity of the Fiji and Tonga archipelagos, the center of the SPO, and the Equatorial HNLC area (see the World Meteorological Organisation numbers in Supplementary Table S1). All the floats are equipped with a Sea-Bird Scientific SBE41 CTD sensor measuring temperature (T), salinity (S), and pressure (P), a Sea-Bird ECO Puck that measures Chlorophyll-*a* fluorescence (excitation/emission wavelengths of 470/695 nm) and the particulate backscattering coefficient at 700 nm (b_{bp}), a Sea-Bird OCR-504 multispectral radiometer that measures the Photosynthetic Available Radiation (PAR) as well as the downwelling irradiance at 380 nm, $E_d(380)$, 412 nm, $E_d(412)$, and 490 nm, $E_d(490)$. Apart from two floats in O_{center}, all the floats are also equipped with Anderaa optodes measuring dissolved oxygen concentration.

The Chlorophyll-*a* fluorescence and b_{bp} coefficient were derived from the raw optical signal of the ECO sensor following the standard BGC-Argo protocol (Carval et al., 2018; Dall'Olmo et al., 2023; Schmechtig et al., 2015, 2023). To account and correct for the strong regional variability in the fluorescence-to-Chl ratio (Petit et al., 2022; Roesler et al., 2017), we assessed a conversion factor for each vertical profiles using the $E_d(490)$ measurements as described by Xing et al. (2011). Each float was attributed a constant correction factor, corresponding to the median values obtained over its lifetime. The resulting factors are consistent with (Roesler et al., 2017 and Petit et al., 2022) in the SPSG. Finally, the Chl profiles were smoothed with a 10-m moving average and corrected from Non-Photochemical Quenching (NPQ) following Terrats et al. (2020). Spikes potentially associated with particle aggregates or zooplankton may be observed in b_{bp} profiles (Briggs et al., 2011; Haëntjens et al., 2020). A 10-m moving average was

applied to the b_{bp} individual profiles, and values exceeding the 5th and 95th percentiles of the residuals were removed, following Barbieux et al. (2019).

The PAR profiles were corrected from cloud effects which intermittently reduces irradiance values. To do so, an envelope was derived for each log-transformed PAR profile, using strictly decreasing and moving-average filters with a 50-m window. The difference between observations and the envelope was used with a threshold to identify the occurrence of clouds. Finally, following Organelli et al. (2016), a 4^{th}-degree beta-spline curve was fitted to the observations not affected by clouds (see details in Supplementary section S2).

For most of the floats used in this study, the profiling frequency is 5 days. However, some of the floats cycled at a higher frequency (1 to 3 days) during a few months after deployment. In this case, only the profiles acquired every 5 days are considered for consistency.

2.2 Classification of the Chl vertical profiles

As in Mignot et al. (2011), two mathematical functions illustrating two main types of Chl vertical profiles — Bloom and SCM — are adjusted to the BGC-Argo Chl profiles (see Supplementary section S3). The SCM type is characterised by a pronounced subsurface peak, while the Bloom type shows elevated values in the upper layer without a significant subsurface peak. Then, the quality of each fit is assessed using the squared Pearson correlation coefficient, r^2, and the Chl profiles are attributed the Bloom or SCM types according to the best statistics. In addition, we include a Hybrid type for the Chl profiles for which both functions have satisfying fits (i.e. $r^2 > 0.8$). This type corresponds to profiles featuring significant surface values with, nonetheless, a notable subsurface maximum. Finally, the Chl profiles for which the fit scores are too low ($r^2 < 0.8$) for both models are classified as Other and discarded (less than 1%). As a result, 12% of the profiles belong to the Bloom type, 75% to the SCM type and 12% to the Hybrid type.

This approach also allows the retrieval of the SCM depth (Z_{SCM}) and width (W_{SCM}) for the Chl profiles of the SCM type, as adjustment parameters of the gaussian model (see Supplementary section S3). The Chl profiles from the SCM type are further classified in two subcategories to determine whether the SCM is related to the occurrence of a carbon biomass maximum

concomitant with the Chl maximum (i.e., Subsurface Biomass Maximum, SBM) or to photoacclimation of phytoplankton cells to low light conditions at depth (i.e., Subsurface Acclimation Maximum, SAM). Following Cornec et al. (2021), vertical profiles of b_{bp}, which can be used as a proxy for the stock of Particulate Organic Carbon (POC), are considered in addition to the Chl profiles. Correlations between Chl and b_{bp} are calculated along depth over [Z_{SCM}-W_{SCM}; Z_{SCM}+W_{SCM}] for each profile. Significant correlation means that a subsurface local maximum of b_{bp} is detected in the proximity of the Z_{SCM}, thus the SCM is considered as a SBM. Inversely, the SCM is considered as a SAM when there is no significant correlation between Chl and b_{bp}. Hence, this classification yields 4 classes that are Bloom, Hybrid, SAM and SBM, with the last two corresponding to profiles of the SCM type. The full method is detailed in the Supplementary section S4.

2.3 An indicator of the shape of Chl vertical profiles (ζ)

Here we propose a novel indicator, ζ, that provides a synthetic, quantitative view of the spatio-temporal variability of the vertical distribution of Chl at the SPO scale. The method to derive ζ relies on the Principal Component Analysis of the whole dataset of Chl profiles (see Supplementary section S5).

The different values of ζ smoothly connect the sigmoid (reflecting the Bloom type, higher values of ζ) and gaussian shapes (reflecting the SCM type, lower values of ζ), passing through the hybrid class associated with intermediate values of ζ (Figure 1c). Therefore, ζ provides information about SCM characteristics such as Z_{SCM}, W_{SCM}, or even surface and SCM Chl values.

2.4 Hydrological variables

BGC-Argo measurements are used to investigate the physical and biogeochemical mechanisms driving the phytoplankton vertical and seasonal variability. First, the mixed layer depth (MLD) is used to trace the surface-driven mixing. MLD is defined as the depth at which surface density is exceeded by 0.125 $kg.m^{-3}$, a density criterion usually considered in the study region (Ohno et al., 2004; Sauzède et al., 2020; Suga et al., 2004). The potential density is computed using the Gibbs-SeaWater library (McDougall & Barker, 2011). The squared Brunt-Vaisala frequency (N^2,

219 or buoyancy frequency) is also estimated. N^2 is commonly used as an indicator of the ocean
220 stratification (Agustí & Duarte, 1999) and its maximum depth (Z_{N2max}) is a proxy for the
221 pycnocline depth (Lü et al., 2020), more independent from surface properties than MLD
222 (Strutton et al., 2023). It is defined as:

223 $$N^2(z) = -\frac{g}{\rho_0}\,\partial_z\sigma(z)$$

224 with z the depth, g the gravitational acceleration, ρ_0 the mean density of seawater (taken as
225 1025 $kg.m^{-3}$), ∂_z the z-wise derivative operator and σ the potential density referenced to the
226 surface.

227 In regions such as the subtropics, the presence of a surface salinity maximum leads to
228 destabilising the salinity vertical profile. During winter, the convective mixing generates a
229 strongly density-compensated layer at the base of the well-mixed layer. This structure can lead
230 to the occurrence of double-diffusive convection (Kolodziejczyk & Gaillard, 2012, 2013; Yeager
231 & Large, 2007). This phenomenon can be illustrated by the Turner angle (Ruddick, 1983):

232 $$T_u(z) = tan^{-1}\left(\frac{\alpha\partial_z T(z) + \beta\partial_z S(z)}{\alpha\partial_z T(z) - \beta\partial_z S(z)}\right)$$

233 with respectively α and β the sea water thermal expansion and haline contraction coefficients.
234 Values of T_u within ±45° correspond to depths where the water column is stable. $T_u > 45°$
235 indicates that the salinity gradient is more destabilising than the temperature gradient is
236 stabilising. Inversely, $T_u < -45°$ indicates that the temperature gradient is more destabilising
237 than the salinity gradient. The process of double-diffusive convection can occur for $T_u > 71.6°$
238 (Ruddick, 1983). Probability that $\mathcal{P}(T_u > 71.6°)$ is computed considering the mean and standard
239 deviation of T_u, assuming a normal distribution.

240 Light penetration is quantified through the depth of the 20 $\mu mol.quanta.m^{-2}.s^{-1}$ isolume (Z_{iso20})
241 using the PAR data from the BGC-Argo floats, as in Barbieux et al. (2019) and Cornec et al.

(2021). The euphotic depth Z_{eu} is defined as the depth at which PAR is equal to 1% of its surface value.

Lastly, the CANYON-B neural network is applied to pressure, temperature, salinity, oxygen (when available; see Supplementary Table S1), position and date data from the BGC-Argo floats to derive nitrate concentrations (Bittig et al., 2018; Sauzède et al., 2017). The nitracline depth, Z_{nit}, is then calculated as the depth of the 1 µmol.L^{-1} isoline (Cermeño et al., 2008; Lavigne et al., 2015; Sauzède et al., 2020).

For all considered variables, monthly climatologies were derived by monthly averaging the individual profiles.

3 Results and discussion

At the basin scale, the ζ index provides synthetic information about the distinct types of Chl vertical profiles within the SPO (Figure 1a). The lowest seasonal values of ζ ($\simeq$ 0.25), in O_{center} (Figure 1a), are associated with the deepest SCM (down to 140 m) and the lowest surface Chl ($\simeq$ 0.02 mg.m^{-3}; Figure 1c). Intermediate values of ζ ($0.5 < \zeta < 0.7$) can be observed in O_{Coral} and O_{Fiji} reflecting shallower Z_{SCM} (~100 m) and higher surface Chl values (0.05 mg.m^{-3}) along a zonal gradient toward the western oligotrophic area. E_{HNLC} and T_{Tasman} mesotrophic areas are associated with the Bloom and Hybrid classes ($\zeta > 0.85$ and $0.75 < \zeta < 0.85$, respectively). In addition to providing a synoptic view of the SPO spatial variability in the Chl vertical distributions, ζ also allows investigating their seasonal variations.

3.1 The zonal gradient of the South Pacific oligotrophic gyre

In the O_{center} region, the ζ index shows weak, yet notable seasonal variations. Minimum ζ values ($\simeq$0.25, Figure 2a) are observed from September to March and are associated with a deep SCM compared to other oligotrophic regions ($Z_{SCM} \simeq$150 m; Figure 2b). In contrast, maximum ζ values (0.45) are found during the austral winter (July), when the SCM is the shallowest (Z_{SCM} ~125 m). These results are coherent with a permanent SCM regime reported in several previous studies (e.g. Cornec et al., 2021; Dandonneau et al., 2004; Mignot et al., 2014). Here, it is related with a

MLD permanently 100-150 m shallower than Z_{nit} (Figure 2b), illustrating that the seasonal convection cannot reach the nitracline and uplift nutrients toward the upper sunlit layer in this area. Also, seasonal variations of the SCM depth are light-driven as illustrated by a Z_{SCM} closely following Z_{iso20} ($r = 0.93$; Figure 2b; Mignot et al., 2014).

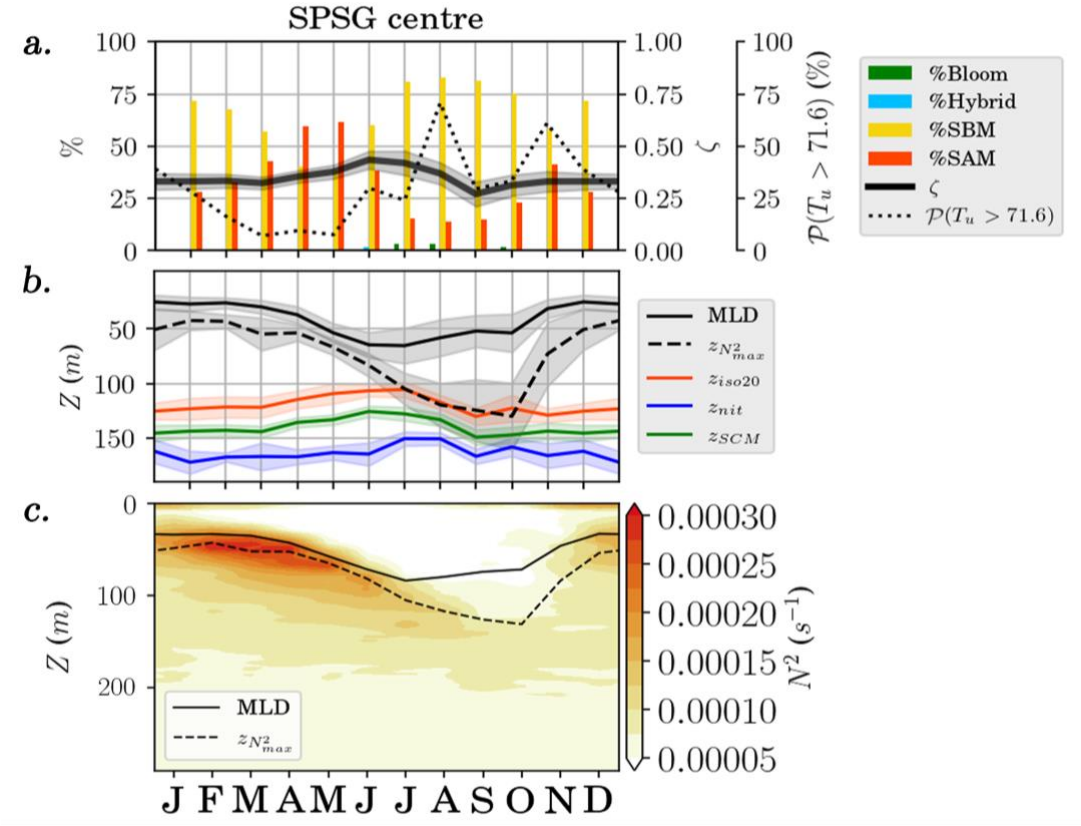

Figure 2. Seasonal climatologies for O_{center} of: (a) the percentage of Chl profile types (Bloom, Hybrid, SBM and SAM; left axis), ζ values (first right axis, solid black line), and probability of T_u being > 71.6 (second right axis, dash black line); (b) MLD, Z_{N2max}, Z_{iso20}, Z_{nit} and Z_{SCM} along depth; (c) N^2 along depth. MLD and Z_{N2max} as in (b) are reported.

Although vertical Chl profiles of the SCM type dominate throughout the year in the O_{center} region, the relative contribution of SAM (induced by photoacclimation) or SBM (associated with an increase in carbon biomass) is highly variable on a seasonal scale. SAM profiles dominate and reach their maximum occurrence frequency (60%) in April-May (late autumn/early winter in the Southern Hemisphere). SBM profiles dominate throughout the rest of the year, with a

maximum contribution (80%) in the July-October period (late winter/spring). These observations contrast with previous studies in permanently stratified oligotrophic regions indicating a dominance of SBM only in summer (December-March) likely due to a Z_{SCM} closer to the nitrate pool following the seasonal isolume deepening (Barbieux et al., 2019; Cornec et al., 2021; Mignot et al., 2014).

To understand the dominance of the SBM class in June-October, we investigate the variations of N^2 which provides additional information about stratification and vertical stability of the water column (Figure 2c). Indeed, O_{center} has particular hydrodynamic properties as the South Pacific Tropical Water (SPTW) is characterised by a vertical salinity maximum (35.6 - 36.5 psu) located at 8°S - 25°S, 160°W - 110°W, lying in the upper thermocline around the 1025 $kg.m^{-3}$ isopycnal (Qu et al., 2013; Tsuchiya & Talley, 1996). In winter/spring, stratification weakens (Figure 2c) and the depth of its maximum Z_{N2max} deepens well below the MLD (Figures 2b, 2c). This suggests stronger convection and vertical mixing leading to the formation of density-compensated layers between the base of the ML and the pycnocline (Kolodziejczyk & Gaillard, 2013; Yeager & Large, 2007). Enhanced vertical mixing may erode the nitracline and allow nutrient diffusion at these depths (although mixing may not be strong enough to extend up to the surface). In addition, an enhanced compensated layer is likely to favour double diffusive mixing (of nutrients) as supported by the values of the Turner angle (high percentage of values > 71.6). This ensemble of processes could explain the significant occurrence of SBM, which would rely on local vertical supply of nutrients.

Oligotrophic characteristics are also found in the O_{Fiji} and O_{Coral} regions. The seasonal variations of ζ follow those of Z_{SCM} (Figures 3a, b), and the MLD remains 70-100 m above Z_{nit} (Figures 3c, d). However, from O_{Center} to O_{Fiji} and O_{Coral}, both Z_{nit} and Z_{iso20} are uplifted and get closer to each other, inducing a Z_{SCM} 30 to 40 m shallower in O_{Coral} than O_{center}. In addition, the westward deepening in the SPO of the tropical-subtropical pycnocline (Johnson & McPhaden, 1999) and Z_{N2max} combined with shallower Z_{nit} could explain stronger nutrient input at Z_{SCM} inducing a higher dominance of SBM. Finally, nutrient injection occurs in the surface layer in August and September when the stratification is the weakest and Z_{N2max} deepens below Z_{nit}. This injection

induces the appearance of Bloom and Hybrid type profiles. The sporadic occurrence of the Hybrid and Bloom types among the other months of the year may rather reflect the supply of nutrients from a relatively shallow Z_{nit} associated with specific phenomena such as the influence of Pacific islands (Messié et al., 2020, 2022), hydrothermal sources supplying iron as reported in O_{Fiji} (Guieu et al., 2018; Tilliette et al., 2022), or eddies and front activity (Heywood et al., 1996; Travis & Qiu, 2020).

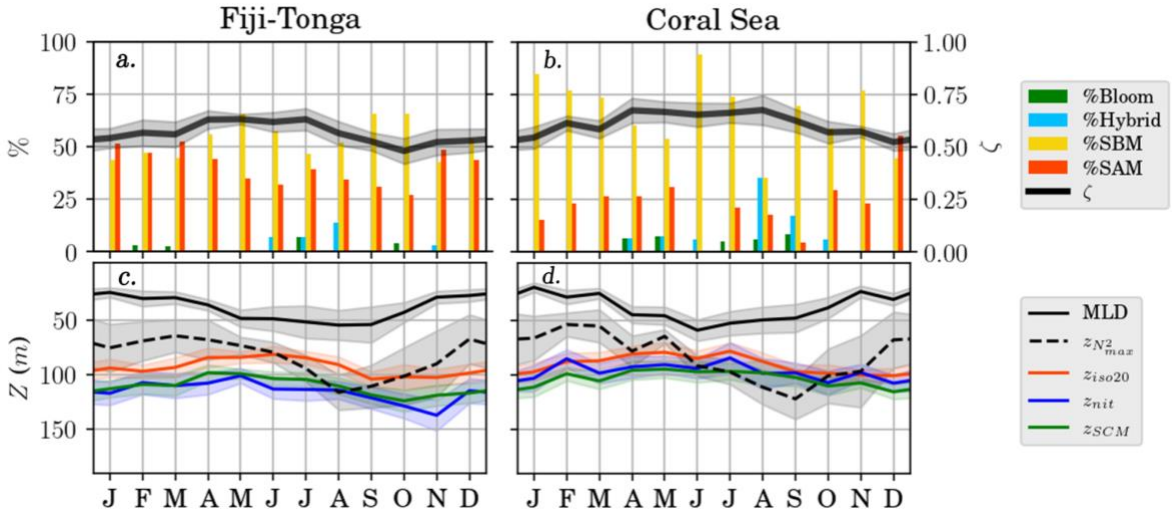

Figure 3. Upper row: same as in Figure 2a without the information on T_u. Lower row: same as in Figure 2b for O_{Fiji} (left column) and O_{Coral} (right column).

3.2 The productive mid-latitude Tasman Sea and equatorial HNLC area

At temperate latitudes, the elevation of Chl in the Tasman front is partly related to the mixing of relatively warm, macronutrient-poor but iron-rich oligotrophic water from the subtropics with cooler, macronutrient-rich but iron-poor subantarctic water (Boyd et al., 1999). In this region, the ζ index reaches high values (0.75 - 0.9) compared to the overall low values found in the three oligotrophic regions (Figure 4a). From January to April, the predominance of the SCM type profiles reflects a southward shift of the front and a positioning of the floats in an oligotrophic environment with MLDs shallower than Z_{nit} (Figure 4b and Supplementary Figure S6.1a). The predominance of SBM is explained by Z_{nit} and Z_{iso20} approximately located at the same depth. From March to October, the Tasman front has moved northward and the floats are

located in a mesotrophic environment (Supplementary Figure S6.1b and S6.1c). The predominance of the Bloom type profiles reflects two dynamical processes. First, the occurrence of a fall bloom which coincides with the gradual deepening (April to June) of the mixed layer (Supplementary Figure S6.2). Then, the spring bloom coincides with the shoaling of the MLD from August to November. These blooms and MLD dynamics coincide with the surface Chl seasonal variability reported by Tilburg et al. (2002) from three years of satellite observations in the Tasman Sea over 37°S-42°S. Finally, as the Tasman front moves southward at the end of the year, the successive changes of dominance from Bloom to Hybrid, then to SCM type profiles (beginning of the year) illustrate the transition from a mesotrophic to oligotrophic environment.

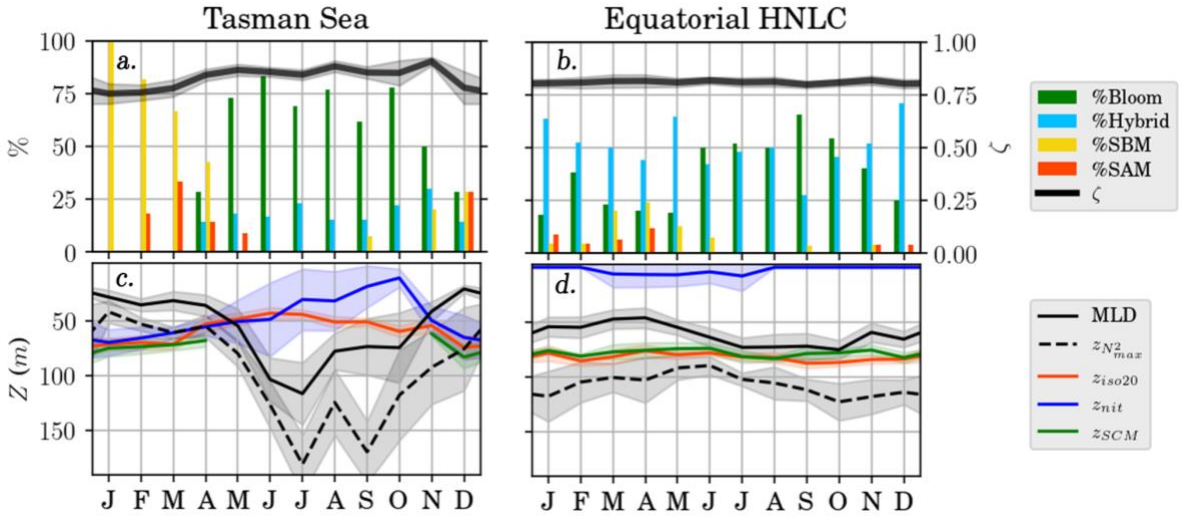

Figure 4. As in Figure 3 but for (a-c) T_{Tasman}, and (b-d) E_{HNLC}.

The E_{HNLC} area is also related to a productive regime with ζ values about 0.8, reflecting Hybrid and Bloom type profiles, and very few occurrences of the SCM type (Figure 4c). Unlike in the Tasman Sea, Z_{nit} either reaches or is close to the surface, highlighting the expected no-limiting nitrate conditions (Figure 4d). Hybrid type profiles dominate all over the year. The consumption of nitrates at the surface could explain the low Chl values ($\simeq$0.2 mg.m^{-3}) consistent with satellite observations, while the SCM-like shape below reflects higher Chl as nitrate concentrations increase with depth. The trajectories of the four floats, mainly upstream of the

Marquesas archipelago, suggest that these types of Chl profiles are related to the regional HNLC environment, rather than to the local Marquesas IME. Finally, the Bloom type profiles occurrence increases from July to November following the seasonal deepening of the MLD, and a subsequent stronger input of nutrients toward the mixed layer. Conversely, the SBM type occasionally occurs in March and April when the MLD is the shallowest.

4 Conclusions

This study provides the first seasonal climatology of Chl vertical distribution in the South Pacific Ocean using BGC-Argo profiling floats. By refining previous general classification methods (based on distinction between Bloom profiles and Subsurface Chlorophyll Maxima profiles, SCM), it also includes distinctions between SCM profiles driven by photoacclimation (SAM), actual biomass increase (SBM), and Hybrid types (intermediate between SCM and Bloom profiles), along with a new index (ζ) for profile shape comparison. The results reveal a permanent deep SCM in the oligotrophic O_{center}, O_{Fiji}, and O_{Coral} regions. A north-westward gradient is observed, with an uplift of the nitracline and SCM depths and a deepening pycnocline leading to increased SBM and hybrid profiles in the west. In the Tasman Sea, contrasting oligotrophic and mesotrophic environments show SBM and Bloom dominance north and south of the Tasman front, respectively, while the high occurrence of Hybrid profiles in E_{HNLC} is linked to the regional HNLC environment rather than local island effects.

Stratification-related metrics (e.g., N^2 and Z_{N2max} indices) appear to better explain the difference in seasonal occurrence of SAM and SBM profiles, compared to the dynamics of the Mixed Layer Depth alone, with vertical mixing and potential double-diffusion events playing key roles in the vertical nutrient inputs from depth toward upper layers.

These findings underscore the need to distinguish between SBM and SAM processes, as SBM-dominated profiles, potentially associated with increased biological production, are more frequent in these oligotrophic regions than previously reported. Expanding in-situ observations in the SPO is critical for understanding long-term changes in primary production and carbon export in response to ongoing and future climate warming.

Funding

The deployments of all the floats (except in the Tasman Sea) have been supported by the French oceanographic fleet.

This work was supported by INSU LEFE Cyber within the framework of the Moana Maty project, as well as the government of French Polynesia for the financial support of the Moana O Te Ati Enana project (convention °07498°).

We would like to thank the Government of French Polynesia and the French State for providing funding support to the THOT project (Contrat de projets Etat-Pays, convention n°8690/MSR/REC, and arrêté de subvention n° HC/2860/DIE/BPT)

The T. Hermilly PhD grant was co-funded by a doctoral research grant from the French Brittany region (Allocations de recherche doctorale, ARED) and the French National Research institute for sustainable Development (IRD).

M.Cornec. was supported by the National Science Foundation (award: OCE 2023274/2147809 to A.J. Fassbender), National Oceanic and Atmospheric Administration (NOAA) Global Ocean Monitoring and Observing program, and NOAA Pacific Marine Environmental Laboratory.

Acknowledgments

The authors would like to thank the following research projects: THOT (Tahitian Ocean Time-series), OUTPACE (Oligotrophy from Ultra-oligoTrophy PACific Experiment), MOANA MATY and Moana O Te Ati Enana cruises, and TONGA (shallow hydroThermal sOurces of trace elemeNts - potential impacts on the biological productivity and bioloGicAl carbon pump) which received BGC-Argo floats from the LEFE GMMC (INSU-CNRS) as a contribution to the French segment of the BGC-Argo program. REFINE has received funding from the European Research Council (ERC) under the European Union's Horizon 2020 research and innovation programme (grant agreement N° 834177). Argo-2030 has received the support of the French government within the framework of the "Investissements d'avenir" program integrated in France 2030 and

managed by the Agence Nationale de la Recherche (ANR) under the reference "ANR-21-ESRE-0019".

Data availability statement

The BGC-Argo data were collected and made freely available by the International Argo Program and the national programs that contribute to it (http://www.argo.ucsd.edu, http://argo.jcommops.org/). This Argo Program is part of the Global Ocean Observing System. All analyses have been performed using python 3.11.3. The code behind the CANYON-B estimation of nitrate from temperature, salinity and oxygen concentration is available openly at https://github.com/HCBScienceProducts/CANYON-B.

References

Agustí, S., & Duarte, C. M. (1999). Phytoplankton chlorophyll a distribution and water column stability in the central Atlantic Ocean. *Oceanologica Acta*, *22*(2), 193–203. https://doi.org/10.1016/S0399-1784(99)80045-0

Baird, M. E., Timko, P. G., Middleton, J. H., Mullaney, T. J., Cox, D. R., & Suthers, I. M. (2008). Biological properties across the Tasman Front off southeast Australia. *Deep Sea Research Part I: Oceanographic Research Papers*, *55*(11), 1438–1455. https://doi.org/10.1016/j.dsr.2008.06.011

Barbieux, M., Uitz, J., Gentili, B., Pasqueron de Fommervault, O., Mignot, A., Poteau, A., Schmechtig, C., Taillandier, V., Leymarie, E., Penkerc'h, C., D'Ortenzio, F., Claustre, H., & Bricaud, A. (2019). Bio-optical characterization of subsurface chlorophyll maxima in the Mediterranean Sea from a Biogeochemical-Argo float database. *Biogeosciences*, *16*(6), 1321–1342. https://doi.org/10.5194/bg-16-1321-2019

Barbieux, M., Uitz, J., Mignot, A., Roesler, C., Claustre, H., Gentili, B., Taillandier, V., D'Ortenzio, F., Loisel, H., Poteau, A., Leymarie, E., Penkerc'h, C., Schmechtig, C., & Bricaud, A. (2022). Biological production in two contrasted regions of the Mediterranean Sea during the oligotrophic period: An estimate based on the diel cycle of optical properties measured by BioGeoChemical-Argo profiling floats. *Biogeosciences*, *19*(4), 1165–1194. https://doi.org/10.5194/bg-19-1165-2022

Bittig, H. C., Steinhoff, T., Claustre, H., Fiedler, B., Williams, N. L., Sauzède, R., Körtzinger, A., & Gattuso, J.-P. (2018). An Alternative to Static Climatologies: Robust Estimation of Open Ocean CO2 Variables and Nutrient Concentrations From T, S, and O2 Data Using Bayesian Neural Networks. *Frontiers in Marine Science*, *5*, 328. https://doi.org/10.3389/fmars.2018.00328

Bock, N., Cornec, M., Claustre, H., & Duhamel, S. (2022). Biogeographical Classification of the Global Ocean From BGC-Argo Floats. *Global Biogeochemical Cycles*, *36*(6), e2021GB007233. https://doi.org/10.1029/2021GB007233

Bonnet, S., Guieu, C., Taillandier, V., Boulart, C., Bouruet-Aubertot, P., Gazeau, F., Scalabrin, C., Bressac, M., Knapp, A. N., Cuypers, Y., González-Santana, D., Forrer, H. J., Grisoni, J.-M.,

Grosso, O., Habasque, J., Jardin-Camps, M., Leblond, N., Le Moigne, F. A. C., Lebourges-Dhaussy, A., … Tilliette, C. (2023). Natural iron fertilization by shallow hydrothermal sources fuels diazotroph blooms in the ocean. *Science*, *380*(6647), 812–817. https://doi.org/10.1126/science.abq4654

Boyd, P., LaRoche, J., Gall, M., Frew, R., & McKay, R. M. L. (1999). Role of iron, light, and silicate in controlling algal biomass in subantarctic waters SE of New Zealand. *Journal of Geophysical Research: Oceans*, *104*(C6), 13395–13408. https://doi.org/10.1029/1999JC900009

Briggs, N., Perry, M. J., Cetinić, I., Lee, C., D'Asaro, E., Gray, A. M., & Rehm, E. (2011). High-resolution observations of aggregate flux during a sub-polar North Atlantic spring bloom. *Deep Sea Research Part I: Oceanographic Research Papers*, *58*(10), 1031–1039. https://doi.org/10.1016/j.dsr.2011.07.007

Carval, T., Coatanoan, C., Schmechtig, C., Racape, V., Rannou, J. P., & Dobler, D. (2018). *Processing Bio-Argo particle backscattering at the DAC level* (Version 1.4) [Pdf]. Ifremer. https://doi.org/10.13155/39459

Cermeño, P., Dutkiewicz, S., Harris, R. P., Follows, M., Schofield, O., & Falkowski, P. G. (2008). The role of nutricline depth in regulating the ocean carbon cycle. *Proceedings of the National Academy of Sciences*, *105*(51), 20344–20349. https://doi.org/10.1073/pnas.0811302106

Chiswell, S. M., Bradford-Grieve, J., Hadfield, M. G., & Kennan, S. C. (2013). Climatology of surface chlorophyll a, autumn-winter and spring blooms in the southwest Pacific Ocean. *Journal of Geophysical Research: Oceans*, *118*(2), 1003–1018. https://doi.org/10.1002/jgrc.20088

Claustre, H., & Maritorena, S. (2003). The Many Shades of Ocean Blue. *Science*, *302*(5650), 1514–1515. https://doi.org/10.1126/science.1092704

Claustre, H., Sciandra, A., & Vaulot, D. (2008). Introduction to the special section bio-optical and biogeochemical conditions in the South East Pacific in late 2004: The BIOSOPE program. *Biogeosciences*, *5*(3), 679–691. https://doi.org/10.5194/bg-5-679-2008

Cornec, M., Claustre, H., Mignot, A., Guidi, L., Lacour, L., Poteau, A., D'Ortenzio, F., Gentili, B., & Schmechtig, C. (2021). Deep Chlorophyll Maxima in the Global Ocean: Occurrences, Drivers and Characteristics. *Global Biogeochemical Cycles*, *35*(4), e2020GB006759. https://doi.org/10.1029/2020GB006759

Cullen, J. J. (2015). Subsurface Chlorophyll Maximum Layers: Enduring Enigma or Mystery Solved? In *Annual Review of Marine Science* (Vol. 7, Issue Volume 7, 2015, pp. 207–239). Annual Reviews. https://doi.org/10.1146/annurev-marine-010213-135111

Dall'Olmo, G., Bhaskar Tvs, U., Bittig, H., Boss, E., Brewster, J., Claustre, H., Donnelly, M., Maurer, T. L., Nicholson, D., Paba, V., Plant, J. N., Poteau, A., Sauzède, R., Schallenberg, C., Schmechtig, C., Schmid, C., & Xing, X. (2023). *BGC Argo quality control manual for particles backscattering* (Version 1.0) [Pdf]. Ifremer. https://doi.org/10.13155/60262

Dandonneau, Y., Deschamps, P.-Y., Nicolas, J.-M., Loisel, H., Blanchot, J., Montel, Y., Thieuleux, F., & Bécu, G. (2004). Seasonal and interannual variability of ocean color and composition of phytoplankton communities in the North Atlantic, equatorial Pacific and South Pacific. *Deep Sea Research Part II: Topical Studies in Oceanography*, *51*(1), 303–318. https://doi.org/10.1016/j.dsr2.2003.07.018

Doty, M. S., & Oguri, M. (1956). The Island Mass Effect. *ICES Journal of Marine Science*, *22*(1), 33–37. https://doi.org/10.1093/icesjms/22.1.33

Ellwood, M. J., Law, C. S., Hall, J., Woodward, E. M. S., Strzepek, R., Kuparinen, J., Thompson, K., Pickmere, S., Sutton, P., & Boyd, P. W. (2013). Relationships between nutrient stocks and inventories and phytoplankton physiological status along an oligotrophic meridional transect in the Tasman Sea. *Deep Sea Research Part I: Oceanographic Research Papers*, *72*, 102–120. https://doi.org/10.1016/j.dsr.2012.11.001

Eppley, R. W., Renger, E. H., & Harrison, W. G. (1979). Nitrate and phytoplankton production in southern California coastal waters1. *Limnology and Oceanography*, *24*(3), 483–494. https://doi.org/10.4319/lo.1979.24.3.0483

Gačić, M., Civitarese, G., Miserocchi, S., Cardin, V., Crise, A., & Mauri, E. (2002). The open-ocean convection in the Southern Adriatic: A controlling mechanism of the spring

494 phytoplankton bloom. *Continental Shelf Research*, *22*(14), 1897–1908.
495 https://doi.org/10.1016/S0278-4343(02)00050-X
496 Geider, R. J. (1987). Light and temperature dependence of the carbon to chlorophyll a ratio in
497 microalgae and cyanobacteria: Implications for physiology and growth of
498 phytoplankton. *New Phytologist*, *106*(1), 1–34. https://doi.org/10.1111/j.1469-
499 8137.1987.tb04788.x
500 Guieu, C., Bonnet, S., Petrenko, A., Menkes, C., Chavagnac, V., Desboeufs, K., Maes, C., &
501 Moutin, T. (2018). Iron from a submarine source impacts the productive layer of the
502 Western Tropical South Pacific (WTSP). *Scientific Reports*, *8*(1), 9075.
503 https://doi.org/10.1038/s41598-018-27407-z
504 Haëntjens, N., Della Penna, A., Briggs, N., Karp-Boss, L., Gaube, P., Claustre, H., & Boss, E.
505 (2020). Detecting Mesopelagic Organisms Using Biogeochemical-Argo Floats.
506 *Geophysical Research Letters*, *47*(6), e2019GL086088.
507 https://doi.org/10.1029/2019GL086088
508 Johnson, G. C., & McPhaden, M. J. (1999). Interior Pycnocline Flow from the Subtropical to the
509 Equatorial Pacific Ocean*. *Journal of Physical Oceanography*, *29*(12), 3073–3089.
510 https://doi.org/10.1175/1520-0485(1999)029<3073:IPFFTS>2.0.CO;2
511 Kerry, C., & Roughan, M. (2020). Downstream Evolution of the East Australian Current System:
512 Mean Flow, Seasonal, and Intra-annual Variability. *Journal of Geophysical Research:*
513 *Oceans*, *125*(5), e2019JC015227. https://doi.org/10.1029/2019JC015227
514 Kolodziejczyk, N., & Gaillard, F. (2012). Observation of spiciness interannual variability in the
515 Pacific pycnocline. *Journal of Geophysical Research: Oceans*, *117*(C12), 2012JC008365.
516 https://doi.org/10.1029/2012JC008365
517 Kolodziejczyk, N., & Gaillard, F. (2013). Variability of the Heat and Salt Budget in the Subtropical
518 Southeastern Pacific Mixed Layer between 2004 and 2010: Spice Injection Mechanism.
519 *Journal of Physical Oceanography*, *43*(9), 1880–1898. https://doi.org/10.1175/JPO-D-13-
520 04.1
521 Lacour, L., Briggs, N., Claustre, H., Ardyna, M., & Dall'Olmo, G. (2019). The Intraseasonal
522 Dynamics of the Mixed Layer Pump in the Subpolar North Atlantic Ocean: A

Biogeochemical-Argo Float Approach. *Global Biogeochemical Cycles*, *33*(3), 266–281. https://doi.org/10.1029/2018GB005997

Lavigne, H., D'Ortenzio, F., Ribera D'Alcalà, M., Claustre, H., Sauzède, R., & Gacic, M. (2015). On the vertical distribution of the chlorophyll a concentration in the Mediterranean Sea: A basin-scale and seasonal approach. *Biogeosciences*, *12*(16), 5021–5039. https://doi.org/10.5194/bg-12-5021-2015

Lewis, M. R., Hebert, D., Harrison, W. G., Platt, T., & Oakey, N. S. (1986). Vertical Nitrate Fluxes in the Oligotrophic Ocean. *Science*, *234*(4778), 870–873. https://doi.org/10.1126/science.234.4778.870

Lü, H., Zhao, X., Sun, J., Zha, G., Xi, J., & Cai, S. (2020). A case study of a phytoplankton bloom triggered by a tropical cyclone and cyclonic eddies. *PLOS ONE*, *15*(4), 1–18. https://doi.org/10.1371/journal.pone.0230394

Martinez, E., & Maamaatuaiahutapu, K. (2004). Island mass effect in the Marquesas Islands: Time variation. *Geophysical Research Letters*, *31*(18). https://doi.org/10.1029/2004GL020682

Martinez, E., Rodier, M., Pagano, M., & Sauzède, R. (2020). Plankton spatial variability within the Marquesas archipelago, South Pacific. *Journal of Marine Systems*, *212*, 103432. https://doi.org/10.1016/j.jmarsys.2020.103432

McDougall, T. J., & Barker, P. M. (2011). *Getting started with TEOS-10 and the Gibbs Seawater (GSW) Oceanographic Toolbox*.

Messié, M., Petrenko, A., Doglioli, A. M., Aldebert, C., Martinez, E., Koenig, G., Bonnet, S., & Moutin, T. (2020). The Delayed Island Mass Effect: How Islands can Remotely Trigger Blooms in the Oligotrophic Ocean. *Geophysical Research Letters*, *47*(2), e2019GL085282. https://doi.org/10.1029/2019GL085282

Messié, M., Petrenko, A., Doglioli, A. M., Martinez, E., & Alvain, S. (2022). Basin-scale biogeochemical and ecological impacts of islands in the tropical Pacific Ocean. *Nature Geoscience*, *15*(6), 469–474. https://doi.org/10.1038/s41561-022-00957-8

Mignot, A., Claustre, H., D'Ortenzio, F., Xing, X., Poteau, A., & Ras, J. (2011). From the shape of the vertical profile of in vivo fluorescence to Chlorophyll-a concentration. *Biogeosciences*, *8*(8), 2391–2406. https://doi.org/10.5194/bg-8-2391-2011

Mignot, A., Claustre, H., Uitz, J., Poteau, A., D'Ortenzio, F., & Xing, X. (2014). Understanding the seasonal dynamics of phytoplankton biomass and the deep chlorophyll maximum in oligotrophic environments: A Bio-Argo float investigation. *Global Biogeochemical Cycles*, *28*(8), 856–876. https://doi.org/10.1002/2013GB004781

Moore, C. M., Mills, M. M., Arrigo, K. R., Berman-Frank, I., Bopp, L., Boyd, P. W., Galbraith, E. D., Geider, R. J., Guieu, C., Jaccard, S. L., Jickells, T. D., La Roche, J., Lenton, T. M., Mahowald, N. M., Marañón, E., Marinov, I., Moore, J. K., Nakatsuka, T., Oschlies, A., … Ulloa, O. (2013). Processes and patterns of oceanic nutrient limitation. *Nature Geoscience*, *6*(9), 701–710. https://doi.org/10.1038/ngeo1765

Morel, A., Claustre, H., & Gentili, B. (2010). The most oligotrophic subtropical zones of the global ocean: Similarities and differences in terms of chlorophyll and yellow substance. *Biogeosciences*, *7*(10), 3139–3151. https://doi.org/10.5194/bg-7-3139-2010

Moutin, T., Doglioli, A. M., de Verneil, A., & Bonnet, S. (2017). Preface: The Oligotrophy to the UlTra-oligotrophy PACific Experiment (OUTPACE cruise, 18 February to 3 April 2015). *Biogeosciences*, *14*(13), 3207–3220. https://doi.org/10.5194/bg-14-3207-2017

Murray, J., Leinen, M., Feely, R., Toggweiler, R., & Wanninkhof, R. (1992). EqPac: A Process Study in the Central Equatorial Pacific. *Oceanography*, *5*(3), 134–142. https://doi.org/10.5670/oceanog.1992.01

Ohno, Y., Kobayashi, T., Iwasaka, N., & Suga, T. (2004). The mixed layer depth in the North Pacific as detected by the Argo floats. *Geophysical Research Letters*, *31*(11), 2004GL019576. https://doi.org/10.1029/2004GL019576

Oke, P. R., Pilo, G. S., Ridgway, K., Kiss, A., & Rykova, T. (2019). A search for the Tasman Front. *Journal of Marine Systems*, *199*, 103217. https://doi.org/10.1016/j.jmarsys.2019.103217

Organelli, E., Claustre, H., Bricaud, A., Schmechtig, C., Poteau, A., Xing, X., Prieur, L., D'Ortenzio, F., Dall'Olmo, G., & Vellucci, V. (2016). A Novel Near-Real-Time Quality-Control Procedure for Radiometric Profiles Measured by Bio-Argo Floats: Protocols and

Performances. *Journal of Atmospheric and Oceanic Technology*, *33*(5), 937–951. https://doi.org/10.1175/JTECH-D-15-0193.1

Peeters, F., Kerimoglu, O., & Straile, D. (2013). Implications of seasonal mixing for phytoplankton production and bloom development. *Theoretical Ecology*, *6*(2), 115–129. https://doi.org/10.1007/s12080-012-0164-2

Petit, F., Uitz, J., Schmechtig, C., Dimier, C., Ras, J., Poteau, A., Golbol, M., Vellucci, V., & Claustre, H. (2022). Influence of the phytoplankton community composition on the in situ fluorescence signal: Implication for an improved estimation of the chlorophyll-a concentration from BioGeoChemical-Argo profiling floats. *Frontiers in Marine Science*, *9*, 959131. https://doi.org/10.3389/fmars.2022.959131

Qu, T., Gao, S., & Fine, R. A. (2013). Subduction of South Pacific Tropical Water and Its Equatorward Pathways as Shown by a Simulated Passive Tracer. *Journal of Physical Oceanography*, *43*(8), 1551–1565. https://doi.org/10.1175/JPO-D-12-0180.1

Ras, J., Claustre, H., & Uitz, J. (2008). Spatial variability of phytoplankton pigment distributions in the Subtropical South Pacific Ocean: Comparison between in situ and predicted data. *Biogeosciences*, *5*(2), 353–369. https://doi.org/10.5194/bg-5-353-2008

Roesler, C., Uitz, J., Claustre, H., Boss, E., Xing, X., Organelli, E., Briggs, N., Bricaud, A., Schmechtig, C., Poteau, A., D'Ortenzio, F., Ras, J., Drapeau, S., Haëntjens, N., & Barbieux, M. (2017). Recommendations for obtaining unbiased chlorophyll estimates from in situ chlorophyll fluorometers: A global analysis of WET Labs ECO sensors. *Limnology and Oceanography: Methods*, *15*(6), 572–585. https://doi.org/10.1002/lom3.10185

Ruddick, B. (1983). A practical indicator of the stability of the water column to double-diffusive activity. *Deep Sea Research Part A. Oceanographic Research Papers*, *30*(10), 1105–1107. https://doi.org/10.1016/0198-0149(83)90063-8

Sauzède, R., Bittig, H. C., Claustre, H., Pasqueron De Fommervault, O., Gattuso, J.-P., Legendre, L., & Johnson, K. S. (2017). Estimates of Water-Column Nutrient Concentrations and Carbonate System Parameters in the Global Ocean: A Novel Approach Based on Neural Networks. *Frontiers in Marine Science*, *4*, 128. https://doi.org/10.3389/fmars.2017.00128

608 Sauzède, R., Martinez, E., Maes, C., Fommervault, O. P. de, Poteau, A., Mignot, A., Claustre, H.,
609 Uitz, J., Oziel, L., Maamaatuaiahutapu, K., Rodier, M., Schmechtig, C., & Laurent, V.
610 (2020). Enhancement of phytoplankton biomass leeward of Tahiti as observed by
611 Biogeochemical-Argo floats. *Journal of Marine Systems*, *204*, 103284.
612 https://doi.org/10.1016/j.jmarsys.2019.103284
613 Schmechtig, C., Claustre, H., Poteau, A., D'Ortenzio, F., Schallenberg, C., Trull, T., & Xing, X.
614 (2023). *BGC-Argo quality control manual for the Chlorophyll-A concentration* (Version
615 3.0) [Pdf]. Ifremer. https://doi.org/10.13155/35385
616 Schmechtig, C., Poteau, A., Claustre, H., D'Ortenzio, F., & Boss, E. (2015). *Processing BGC-Argo*
617 *chlorophyll-A concentration at the DAC level* (Version 1.0) [Pdf]. Ifremer.
618 https://doi.org/10.13155/39468
619 Shulenberger, E., & Reid, J. L. (1981). The Pacific shallow oxygen maximum, deep chlorophyll
620 maximum, and primary productivity, reconsidered. *Deep Sea Research Part A.*
621 *Oceanographic Research Papers*, *28*, 901–919. https://doi.org/10.1016/0198-
622 0149(81)90009-1
623 Strom, S. L., & Fredrickson, K. A. (2008). Intense stratification leads to phytoplankton nutrient
624 limitation and reduced microzooplankton grazing in the southeastern Bering Sea. *Deep*
625 *Sea Research Part II: Topical Studies in Oceanography*, *55*(16–17), 1761–1774.
626 https://doi.org/10.1016/j.dsr2.2008.04.008
627 Strutton, P. G., Trull, T. W., Phillips, H. E., Duran, E. R., & Pump, S. (2023). Biogeochemical Argo
628 Floats Reveal the Evolution of Subsurface Chlorophyll and Particulate Organic Carbon in
629 Southeast Indian Ocean Eddies. *Journal of Geophysical Research: Oceans*, *128*(4),
630 e2022JC018984. https://doi.org/10.1029/2022JC018984
631 Suga, T., Motoki, K., Aoki, Y., & Macdonald, A. M. (2004). The North Pacific Climatology of
632 Winter Mixed Layer and Mode Waters. *Journal of Physical Oceanography*, *34*(1), 3–22.
633 https://doi.org/10.1175/1520-0485(2004)034<0003:TNPCOW>2.0.CO;2
634 Suthers, I. M., Young, J. W., Baird, M. E., Roughan, M., Everett, J. D., Brassington, G. B., Byrne,
635 M., Condie, S. A., Hartog, J. R., Hassler, C. S., Hobday, A. J., Holbrook, N. J., Malcolm, H.
636 A., Oke, P. R., Thompson, P. A., & Ridgway, K. (2011). The strengthening East Australian

637 Current, its eddies and biological effects—An introduction and overview. *Deep Sea*
638 *Research Part II: Topical Studies in Oceanography*, *58*(5), 538–546.
639 https://doi.org/10.1016/j.dsr2.2010.09.029
640 Terrats, L., Claustre, H., Cornec, M., Mangin, A., & Neukermans, G. (2020). Detection of
641 Coccolithophore Blooms With BioGeoChemical-Argo Floats. *Geophysical Research*
642 *Letters*, *47*(23), e2020GL090559. https://doi.org/10.1029/2020GL090559
643 Tilburg, C. E., Subrahmanyam, B., & O'Brien, J. J. (2002). Ocean color variability in the Tasman
644 Sea. *Geophysical Research Letters*, *29*(10), 125-1-125–4.
645 https://doi.org/10.1029/2001GL014071
646 Tilliette, C., Taillandier, V., Bouruet-Aubertot, P., Grima, N., Maes, C., Montanes, M., Sarthou,
647 G., Vorrath, M.-E., Arnone, V., Bressac, M., González-Santana, D., Gazeau, F., & Guieu, C.
648 (2022). Dissolved Iron Patterns Impacted by Shallow Hydrothermal Sources Along a
649 Transect Through the Tonga-Kermadec Arc. *Global Biogeochemical Cycles*, *36*(7),
650 e2022GB007363. https://doi.org/10.1029/2022GB007363
651 Tsuchiya, M., & Talley, L. D. (1996). Water-property distributions along an eastern Pacific
652 hydrographic section at 135W. *Journal of Marine Research*, *54*(3).
653 https://elischolar.library.yale.edu/journal_of_marine_research/2191
654 Westberry, T., Behrenfeld, M. J., Siegel, D. A., & Boss, E. (2008). Carbon-based primary
655 productivity modeling with vertically resolved photoacclimation. *Global Biogeochemical*
656 *Cycles*, *22*(2). https://doi.org/10.1029/2007GB003078
657 Xing, X., Morel, A., Claustre, H., Antoine, D., D'Ortenzio, F., Poteau, A., & Mignot, A. (2011).
658 Combined processing and mutual interpretation of radiometry and fluorimetry from
659 autonomous profiling Bio-Argo floats: Chlorophyll a retrieval. *Journal of Geophysical*
660 *Research: Oceans*, *116*(C6). https://doi.org/10.1029/2010JC006899
661 Yeager, S. G., & Large, W. G. (2007). Observational Evidence of Winter Spice Injection. *Journal*
662 *of Physical Oceanography*, *37*(12), 2895–2919. https://doi.org/10.1175/2007JPO3629.1
663